J Nanopart Res (2020) 22: 68
https://doi.org/10.1007/s11051-020-4761-5

RESEARCH PAPER

High-saturation magnetization in small nanoparticles of Fe_3O_4 coated with natural oils

Bruno S. Corrêa · Messias S. Costa · Gabriel A. Cabrera-Pasca · Cleidilane Sena · Rafael H. Holanda Pinto · Ana Paula S. Silva · Raul N. Carvalho Junior · Lina Ishida · Jonathan G. A. Ramon · Rafael S. Freitas · Mitiko Saiki · Izabela T. Matos · Eduardo L. Corrêa · Artur W. Carbonari

Received: 25 April 2019 / Accepted: 24 October 2019 / Published online: 6 March 2020

Abstract The enhancement of nanoparticle's magnetic properties with a suitable coating is the main tool to increase their potential as an effective candidate for applications in different areas, especially in biomedicine. In the work here reported, Fe_3O_4 nanoparticles coated with natural oils were synthesized by iron (III) acetylacetonate thermal decomposition and the effects of the coating on the magnetic properties of these particles have been investigated. The oils were extracted from three Amazon fruits seeds: açaí, ucuúba, and bacaba by CO_2 supercritical extraction process, and the relative percentage composition of fatty acids were determined by gas chromatography. A systematic study of crystalline, morphological, and magnetic properties revealed a saturation magnetization (Ms) enhancement and high values of the anisotropy constant for Fe_3O_4 samples when coated with açaí and ucuúba oils, which present a large percentage of saturated total fatty acid. Our results indicate that nanoparticles with sizes smaller than around 5 nm present Ms values as high as that found for bulk Fe_3O_4 and, consequently, much higher than Ms values for nanoparticles usually coated with oleic acid. The nuclear techniques neutron activation analysis and perturbed angular correlations were used to better characterize the nanoparticles.

Keywords Nanoparticles · Fe_3O_4 · Magnetization · Anisotropy · Magnetic hyperfine field · Synthesis

B. S. Corrêa · M. S. Costa · G. A. Cabrera-Pasca · C. Sena
Faculdade de Ciências Exatas e Tecnologia, Universidade Federal do Pará, Abaetetuba, PA, Brazil

B. S. Corrêa · R. H. Holanda Pinto · A. P. S. Silva · R. N. Carvalho Junior
Universidade Federal do Pará, Belem, PA, Brazil

M. S. Costa · G. A. Cabrera-Pasca · C. Sena · M. Saiki · I. T. Matos · E. L. Corrêa · A. W. Carbonari (✉)
Instituto de Pesquisas Energéticas e Nucleares, Universidade de São Paulo, Sao Paulo, Brazil
e-mail: carbornar@ipen.br

L. Ishida · J. G. A. Ramon · R. S. Freitas
Instituto de Física, Universidade de São Paulo, Sao Paulo, Brazil

Introduction

Magnetic nanoparticles and nanocomposites materials have currently captured attention of researchers from different areas such as chemistry, physics, engineering, pharmaceutical, and medicine. The reason is their great potential to be used in a wide range of biomedical applications such as controlled drug delivery, contrast agents for magnetic resonance imaging (MRI), computed tomography, immobilization and separation of biomolecules, hyperthermia, and biosensors as well as gas sensors and battery applications (Zhang et al. 2007; Cuong et al. 2012; Pistone et al. 2013; Brollo et al. 2014; Chen et al. 2014; Ren et al. 2014; Jiao et al. 2015; Guivar et al. 2015). For these applications, nanoparticles must present high quality in terms of their magnetic properties (superparamagnetic behavior with high magnetic moment saturations is highly desirable), crystallinity, morphology with good dispersion, and

easy reproducibility. Moreover, they must be biocompatible and present low toxicity. Methods for synthesize nanoparticles are generally performed by a chemical route involving the use and manipulation of dangerous chemical materials that produce hazardous and polluting waste, therefore increasing the production costs.

Several high-cost commercial oils are used in the synthesis of nanoparticles, such olylamine, acid oleic, and linoleycol oil. However, over the last few years, great progress has been made in green synthesis methods, with the use of natural agents to achieve small nanoparticles with stable capping. These methods are still under development and have been considered a good experimental procedure to obtain nanoparticles with good stability, segregation, morphology, and reduced size (Iravani 2011; Ahmed et al. 2016; Hussain et al. 2016).

Recently, interesting oils have been extracted from Amazon fruits and have been investigated as potential candidates for several applications. In terms of the fatty acid composition, which depends on the extraction methods, açaí oil presents high proportion of oleic, palmitic, and linoleic acids while ucuúba oil contains high proportion of miristic, lauric, and palmitic acids (Da Rocha Filho et al. 1992; Schauss et al. 2006; Soares et al. 2007). Scientific researches have revealed that açaí presents antioxidant, anti-inflammatory, and antiproliferative properties; cardioprotective activities; and may be used in the treatment of asthma, infectious diseases, and as antioxidant nutraceutical supplements (Holderness et al. 2011; Gordon et al. 2012; Teixeira-Neto et al. 2012; Yamaguchi et al. 2015). Due to their high bioactive compounds content, industries are currently using açaí fruit extracts as food additives, dietary supplements, or cosmetics ingredients (Liao et al. 2013). In the same way, ucuúba butter, oil, resin extract, and roots can also have different medicine applications such as the treatment of colic, inflammation, rheumatism, dyspepsia, liver dysfunction, ulcer, gastritis, and cancer, and, in addition, it has antifungal action and it can also be used in hair treatment (Lopes et al. 1996, 1999; Fregonesi et al. 2009; Hiruma-Lima et al. 2009; Carvalho et al. 2010). Bacaba oil is popularly used in the treatment of pulmonary infections as bronchitis and tuberculosis, and as a purgative. Previous studies have revealed that bacaba fruits are a promising phenolic source and, based on their antioxidant capacity, are good in preventing chronic diseases (Abadio Finco et al. 2012). Therefore, unsaturated fatty acids found in açaí and bacaba oils are important to humans, since they are good energy sources for the metabolic mechanisms as well as for constituting the cellular membranes structure (Costa et al. 2017).

An important application of different commercial natural oils is related to their capping properties that improve the magnetic parameters of nanoparticles or add to them new functionalities. Magnetite (Fe_3O_4) is the magnetic iron oxide commonly used for different applications such as those listed above. It has a cubic inverse spinel structure composed of two different sublattices. The tetrahedral sites (positions 8a, usually named as A sites) of this structure are occupied by Fe^{3+} ions while the octahedral sites (positions 16d named as B sites) are occupied by an equal number of Fe^{2+} and Fe^{3+} ions (Iizumi et al. 1982; O'Neill and Dollase 1994). Parvin et al. (2004) reported that monodisperse Fe_3O_4 nanoparticles with average size of 4 nm synthesized with oleic acid present blocking temperature (T_B) of 20 K at 1000 Oe and saturation magnetization of about 37 emu/g. The investigation of the magnetic properties of Fe_3O_4 nanoparticles coated with oleic and dodecanoic acids did not result in appreciable changes in the general magnetic behavior of the samples (Barbeta et al. 2010). Yuan et al. reported that the presence of different coatings and suspension means could affect the magnetism of the nanoparticle magnetic core (with size around 5 nm) due to the surface spin disorder influenced by the coating absorbance and electric charge (Yuan et al. 2012). Specifically, coating material may interact with the atoms at the magnetic core surface forming a magnetically disordered layer that leads to a reduction in the number of magnetic ions in the core. This magnetic phase reduction is also dependent on the coating material (Yuan et al. 2012; Nemala et al. 2014). Therefore, the coating not only influences nanoparticle morphology and crystallinity but also the magnetic properties, which are very important for technological and biomedical applications.

In this paper, the synthesis and characterization of iron oxide (Fe_3O_4) magnetic nanoparticles coated with oils extracted from Amazon natural fruits are reported. These fruits are easily found in the Amazon rainforest and the extraction and analysis of their oils are here reported too. The Amazon fruit oils were extracted from açaí (*Euterpe oleraceae Mart.*) and bacaba (*Oenocarpusbacaba Mart.*) pulp and ucuúba (*Virolasurinamensis*) seeds. All nanoparticle samples were synthesized by thermal decomposition method.

After synthesis, the structure, morphology, composition, and particle size were investigated by X-ray diffraction (XRD), transmission electron microscopy (TEM), neutron activation analysis (NAA), thermogravimetric analyzes (TGA), and small-angle X-ray scattering (SAXS), respectively. In addition, their local and magnetic properties were investigated by perturbed angular correlation (PAC) spectroscopy, magnetization, and ac susceptibility.

Experimental

Açaí, ucuúba, and bacaba fruits were purchased from the local market in the city of Abaetetuba (state of Pará, Brazil). Açaí berries and bacaba were immersed in water at 50 °C for 900 s; their pulps were then extracted with water in an electric depulper. Ucuúba fruits were peeled manually to remove the seeds. Both açaí and bacaba pulps, as well as ucuúba seeds, were lyophilized (Liotop, model L101, São Paulo, Brazil) and stored at − 25 °C. Particle size was analyzed using Tyler sieves (WS Tyler, USA) − 8 + 42 mesh, and the average particle diameter was determined according to the method presented by the ASABE (1998). Sample density was determined using a helium pycnometer (Quantachrome, model Ultrapyc 1200e, USA), and the moisture was determined by infrared moisture balance (Gehaka, model IV 2500, São Paulo, Brazil). These experiments were carried out in triplicate.

Extraction procedures: CO_2 supercritical extraction (CO_2-SE)

The extraction procedure was performed in the SPE-ED SFE (model 7071, Applied Separations, Allentown, PA, USA) equipped with a compressor (model CSA 7.8, internal volume of 19.7 L, Schuz, SC, Brazil) of CO_2 gas (99% purity, White Martins, PA, Brazil), and a CO_2 flow meter (Alicat Scientific M 5SLPM Tucson, AZ, USA), using a recycled ethylene glycol aqueous solution at − 5 °C (Polyscience F08400796 Nilles, Illinois, USA). The fruit extracts were obtained under the following conditions of temperature and pressure, respectively: 40 °C and 350 bar for ucuúba, 70 °C and 320 bar for açaí in a cylindrical extraction cell of 50 mL volumetric capacity (internal diameter of 0.014 m and height of 0.3248 m), and 40 °C and 290 bar for bacaba in a 100-ml extraction cell (internal diameter of 0.0314 m and height of 0.1244 m) according to the method described by Batista et al. (2016). The CO_2 mass flow rate in all extractions was 8.85×10^{-5} kg/s. The process was divided into two stages: static and dynamic periods of 1800 s and 10,800 s, respectively. All the extractions were performed in duplicate.

Determination of fatty acids in CO_2-SE extracts

The relative percentage composition of fatty acids was determined by conversion into fatty acid methyl esters (FAMEs) according to the method described by Rodrigues et al. (2010). The composition was then determined using a gas chromatograph (Varian model CP 3380) equipped with a flame ionization detector and with a CP-Sil 88 capillary column (length 60 m, internal diameter 0.25 mm, film thickness 0.25 μm; Varian Inc., USA). The gas chromatograph used FID detector and injector (split ratio 1:100) temperatures of 250 °C, an injection volume of 1 μL, and helium as carrier gas at a flow rate of 0.9 mL/min. The column temperature was set to 80 °C for 4 min and increased to 205 °C at a rate of 4 °C/min. The software Varian Star 3.4.1 was used for the chromatograms, and standard fatty acids mixture (Nu-check-prep, Inc., USA) was used to quantify the fatty acids. The fatty acid contents were expressed as total fatty acids relative percentages. These experiments were performed in duplicate.

Synthesis of magnetite nanoparticles

Iron oxide nanoparticle samples were synthesized at IPEN by a modified thermal decomposition method (Oliveira et al. 2011), which consists in dissolving 2 mmol of iron(III) acetylacetonate in 20 mL of diphenylether, 2 mL of ucuúba, bacaba or açaí oil, 4 mmol of oleylamine, and 10 mmol of 1,2-octanediol. Using a round-bottom flask with three necks, one of them connected to a condenser, the mixture was kept under an inert nitrogen atmosphere stirring for 2 h at 258 °C. Specifically in our synthesis, the natural Amazonian fruit oils replaced the usual oleic acid. After cooling at room temperature, particles were purified by centrifugation in ethanol for 30 min. This purification process was performed three times. After drying under low pressure (about 1 kPa) for 24 h, a fine powder was obtained.

Characterization

In order to check nanoparticle crystallinity, X-ray diffraction patterns for each sample were obtained. Measurements were performed using a PANalytical X-ray diffractometer, model X'Pert PRO with X'Celerator detector using the Cu-Kα radiation ($\lambda_{\alpha 1}$ = 0.154060 nm e $\lambda_{\alpha 2}$ = 0.154443 nm) at 40 kV and 40 mA. A step of 0.05° was used for the collection of data. The size and dispersion of nanoparticles after synthesis were determined by small-angle X-ray scattering technique (SAXS), which were performed using a Bruker's NANOSTAR equipment. The incoming monochromatic X-ray beam wavelength was λ = 1.5418 Å (Cu-K_α), and the sample-detector distance was about 0.67 m. The SAXS data were analyzed by the indirect Fourier transformation (IFT) method using GNOM (Svergun 1992) from the ATSAS program suite. We used the IFT method in order to obtain the real-space volume distribution function D_V, which corresponds to a histogram over all the different volumes of hard spheres within the nanoparticle.

Transmission electron microscopy (TEM) images were obtained on a JEOL JEM 2100 microscope operating at an accelerating voltage of 200 kV. Samples for TEM observations were prepared by placing a drop of a toluene solution containing the dispersed nanoparticles on a carbon-coated copper grid. The distribution of the average particle size was estimated through a visual inspection, assuming a spherical shape. These estimations were compared with those from SAXS results.

In order to determine the concentrations of Fe_3O_4 and the capping material in all nanoparticle samples with high precision, neutron activation analysis (NAA) was performed. Measurements of thermogravimetric analysis (TGA) for Fe_3O_4 + ucuúba sample were also taken, and the results were compared with those of NAA. Powder samples of 30.58 mg, 52.05 mg, and 69.10 mg of Fe_3O_4 coated, respectively, with açaí, ucuúba, and bacaba were used for NAA measurements. These samples along with a standard mass of Fe were irradiated for 16 h under a thermal neutron flux of 5.4×10^{12} n.cm^{-2} s^{-1} in the IEA-R1 research reactor of IPEN. After an intentional delay of 1 week, the Fe element was identified in the sample by measuring the gamma energies of 1099.25 keV and 1291.60 keV in the decay of ^{59}Fe (half-life of 44.5 days) using a hyper-pure Ge detector connected to a DSA 1000 Digital Spectrum Analyzer (Canberra model). Taking into account the results of the iron pattern measurements, the concentration of Fe into the samples was then calculated using the comparative method (De Soete et al. 1972), which permitted the determination of the mass of Fe_3O_4 in each sample. The TGA measurements were carried out using thermal analysis equipment (Netzch, model STA 449 F3 Jupiter). About 10 mg of the sample powder was analyzed from room temperature up to 500 °C, with a heating rate of 10 °C/min. The curve of the mass variation as a function of temperature was constructed, as well as its derivative (dm/dT) that was used to identify the thermal events that occurred during the analysis.

Magnetization measurements were carried out using a superconducting quantum interference device (SQUID) magnetometer (Quantum Design MPMS) as a function of the temperature in the zero-field-cooled (ZFC) and field-cooled (FC) procedures. The ZFC curves were obtained by measuring the magnetization during the sample warming after cooling it without applying a magnetic field, and the FC curve is obtained by measuring while cooling the sample in the presence of a magnetic field (H = 100 Oe). Magnetization loops $M(H)$ were measured in the field range ± 7 T at different temperature.

Local crystalline structure and magnetic interactions in all samples after synthesis and after an additional annealing at 973 K for 2.5 h were examined by perturbed gamma-gamma angular correlation (PAC) spectroscopy at IPEN. This nuclear technique is based on hyperfine interaction phenomena and is very useful because it provides valuable information on short-range interactions. This technique has been used with success to investigate different magnetism sources in nanostructured materials (Uhrmacher 2011; Matos et al. 2015; Sales et al. 2017). PAC is sensitive to small distortions in the crystalline structure around a specific site occupied by the probe nucleus as well as the presence of impurities (Ramirez et al. 2015; Sena et al. 2015). In order to carry out PAC measurements, new samples of Fe_3O_4 coated with each natural oil were prepared following the same procedure described above, however, with the addition of a small drop of liquid $^{111}InCl_3$ (corresponding to a very low concentration < 1 ppm) to the starting solution used to synthesize the nanoparticles. Just after the synthesis, part of the resulting powder samples containing the coated nanoparticles was measured by PAC, while another part of each sample was heated at 973 K for 2.5 h in an evacuated quartz tube to remove organic materials and provide

sufficiently energy to increase the probe nuclei fraction into the crystalline core of the nanoparticles.

PAC measurements were carried out at room temperature with a conventional fast-slow coincidence set-up using four BaF_2 detectors. The resulting spin rotation spectra (R(t)) is given by

$$R(t) = A_{22}G_{22}(t) = A_{22}\sum_i f_i G_{22}^i(t) \quad (1)$$

where A_{22} is the unperturbed angular correlation coefficient. $R(t)$ spectra were fitted using theoretical models that take into account the population (f_i) of the site fractions occupied by the probe nuclei, and the nature of the hyperfine interactions, given by the perturbation functions $G_{22}(t)$, which can be magnetic, characterized by the Larmor frequency (ω_L), electric, characterized by the quadrupole frequency (ν_Q) and the asymmetry parameter η, or a combination of both. For magnetic interactions, $G_{22}(t) = 0.2 + 0.4\cos(\omega_L t) + 0.4\cos(2\omega_L t)$, where ω_L is proportional to the hyperfine field (B_{hf}) and it is given by $\omega_L = \mu_N g B_{hf}/\hbar$, where μ_N is nuclear magneton and g is the g-factor ($g = 0.306 \pm 0.001$ for ^{111}Cd probe nuclei). As for electric quadrupole interactions, $G_{22}(t) = S_{20} + \sum_{n=1}^{3} S_{2n}(\eta)\cos[g(\eta)\nu_Q t]$, with the nuclear quadrupole frequency $\nu_Q = eQV_{ZZ}/h$, where Q is the nuclear quadrupole moment and the asymmetry parameter $\eta = (V_{XX} - V_{YY})/V_{ZZ}$, being V_{ZZ} the major component of the electric field gradient (EFG) tensor in its main axis system (Dogra et al. 2001; Bosch-Santos et al. 2015).

Table 1 Fatty acid composition of oils extracted from ucuúba seeds, açaí and bacaba pulps by the supercritical extraction method. Values are in percentage

Fatty acid	Açaí 70 °C/ 320 bar	Ucuúba 40 °C/350 bar	Bacaba 40 °C/290 bar
C8:0	2.27	–	0.06
C10:0	–	0.44	0.01
C12:0	0.33	17.30	0.15
C13:0	0.21	0.17	0.06
C14:0	0.42	77.61	0.40
C15:0	–	1.26	0.06
C16:0	90.86	2.67	22.12
C16:1	0.08	0.31	0.43
C17:0	0.19	–	0.09
C18:0	5.35	0.20	3.39
C18:1	0.23	0.05	61.16
C18:2	–	–	11.48
C18:3	–	–	0.11
C20:0	–	–	0.48
C22:0	–	–	–
Saturated total	99.67	99.64	26.82
Unsaturated total	0.31	0.36	73.18

C8:0 (caprylic acid), C10:0 (capric acid), C12:0 (lauric acid), C13:0 (tridecanoic acid), C14:0 (myristic acid), C15:0 (pentadecanoic acid), C16:0 (palmitic acid), C16:1 (palmitoleic acid), C17:0 (margaric acid), C18:0 (stearic acid); C18:1 (oleic acid), C18:2 (linoleic acid), C18:3 (linolenic acid), C20:0 (arachidic acid), C22:0 (behenic acid)

Results and discussion

Table 1 displays the fatty acid composition determined by gas chromatography for the oils extracted from ucuúba seeds and açaí and bacaba pulps. One can see that açaí oil has 90.86% of palmitic acid (C16:00), 5.35% of stearic acid (C18:00), and 2.27% of caprylic acid (C8:00). The ucuúba oil has 77.61% of myristic acid (C14:00), 17.30% of lauric acid (C12:00), and 2.67% of palmitic acid (C16:00). The bacaba oil has 61.16% of oleic acid (C18:1), 22.12% of palmitic acid (C16:00), and 11.48% of linoleic acid (C18:2). Note that açaí and ucuúba oils have 99.6% of saturated fatty acid while bacaba has 26.8% and 73.2% of saturated and unsaturated fatty acid, respectively.

After synthesis, nanoparticle samples were analyzed by X-ray diffraction (see XRD patterns in Fig. 1a), where 2θ diffraction peaks were observed at 30°, 35.6°, 37.1°, 43°, 53.5°, 57°, and 62.7° corresponding, respectively, to the (220), (311), (222), (400), (422), (511), and (440) Bragg planes. These results observed for all samples reveal a unique phase in agreement with the pattern reported by Shen et al. (2012) and consistent with cubic inverse spinel phase of Fe_3O_4 belonging to $Fd\bar{3}m$ space group and lattice parameter of 8.395 Å. The diffraction peak broadening is a signature of the nanoparticle small size. Additionally, the inset in Fig. 1b shows the SAXS results for all samples. The best fitting has been reached when a poly-dispersed system of spheres with different volumes is considered. The size distribution D_V results (Fig. 1b) reveal that Fe_3O_4 nanoparticles have size distributions centered at a diameter close to 3 nm with a smaller fraction of larger spheres. The average diameters with respective uncertainties

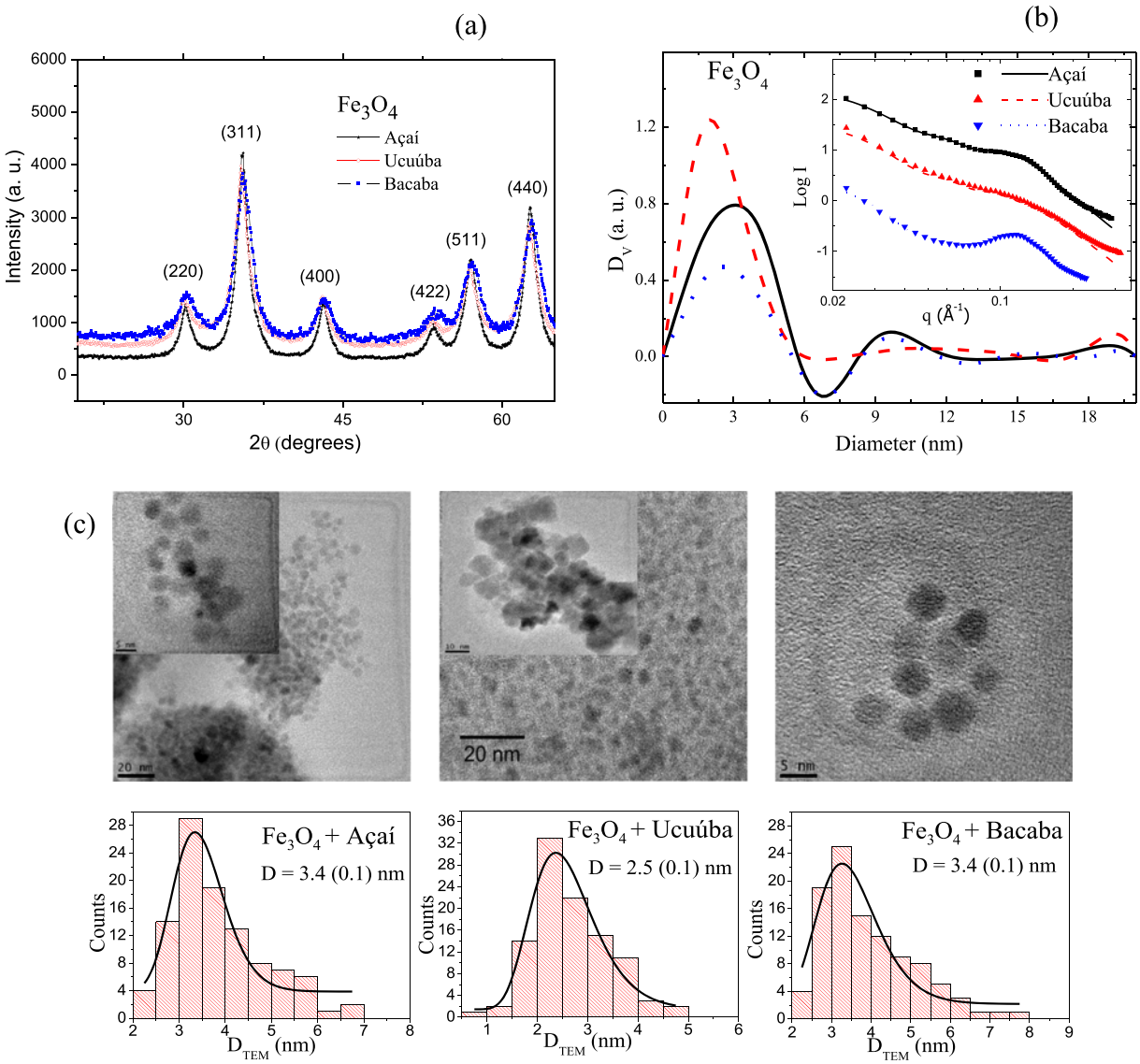

Fig. 1 **a** X-ray diffraction patterns, **b** SAXS results, and **c** TEM images of the synthesized nanoparticles with the corresponding histogram (below each image) fitted with a log-normal distribution (solid line)

obtained from a Gaussian function fit to the highest amplitude Dv peak for each sample are $D_{SAXS} \approx 3.1 \pm 1.7$ nm, 2.0 ± 1.1 nm, and 2.7 ± 1.5 nm for açaí, ucuúba, and bacaba, respectively. Moreover, as revealed for the cross-sectional TEM images in dark contrast, all samples have spherical shape as displayed in Fig. 1c. For Fe_3O_4 + açaí sample, images show particles with 3.4 nm (0.1) average diameter and a small fraction with larger diameter of 5 nm, while Fe_3O_4 + ucuúba and Fe_3O_4 + bacaba samples show particles with average diameter of 2.5 nm (0.1) and 3.4 nm (0.1), respectively. The difference in the diameter values measured by the two methods is due to the larger number of particles that are measured by SAXS than that taken from TEM images. SAXS determine the average size of particles from a quite large number of particles interacting with the incident X-rays.

In order to determine the percentage in weight (%wt) of oxide concentrations for Fe_3O_4 + açaí, Fe_3O_4 + ucuúba, and Fe_3O_4 + bacaba samples, NAA measurements were carried out as described above. The results revealed that the nanoparticle cores are formed by ~

75%, ~ 64%, and ~ 25% of Fe_3O_4, respectively. Consequently, around 25%, 36%, and 75% of the total mass of nanoparticles corresponds to the capping organic material most likely due to the fatty carbonic-acid chains contained in açaí, ucuúba, and bacaba oils, respectively; see the schematic representation at bottom panel in Fig. 2. To verify the NAA results, thermogravimetric analysis (TGA) and the differential thermogravimetric (DTG) measurements were performed in the Fe_3O_4 + ucuúba sample in the temperature range from 25 to 500 °C. Figure 2 displays the DTG and TGA resulting curves. Within the temperature range used, one can observe the degradation of the ucuúba oil occurring in two steps. In the first step, a small loss of mass happens between the temperature range at 25 to 210 °C due to the thermal desorption of fatty acids that compose the ucuúba oil; the second step shows a larger loss of mass between 210 and 450 °C, indicating that the oil has been completely removed/degradated due to the dehydrogenation of the fatty acids (Sahoo et al. 2001; Pérez-Dieste et al. 2003; Zhang et al. 2006). After these TGA steps, around 64% of the total initial mass remained in the sample; therefore, 36% of the total sample mass corresponds to the ucuuba oil that was covering the surface of the nanoparticles. This result is in very good agreement with that of NAA measurements. Consequently, one can consider NAA as good as TGA in determining the analytic mass of the Fe_3O_4 core of nanoparticles. Hence, NAA technique is a very efficient alternative to investigate the mass concentration of Fe_3O_4 nanoparticle samples capped with different materials with the advantage to be a non-destructive technique. For example, the NAA technique was used by Corrêa et al. (2018) to determine the mass of Er in nanoparticles of Er_2O_3 in order to normalize the magnetization values (Corrêa et al. 2018).

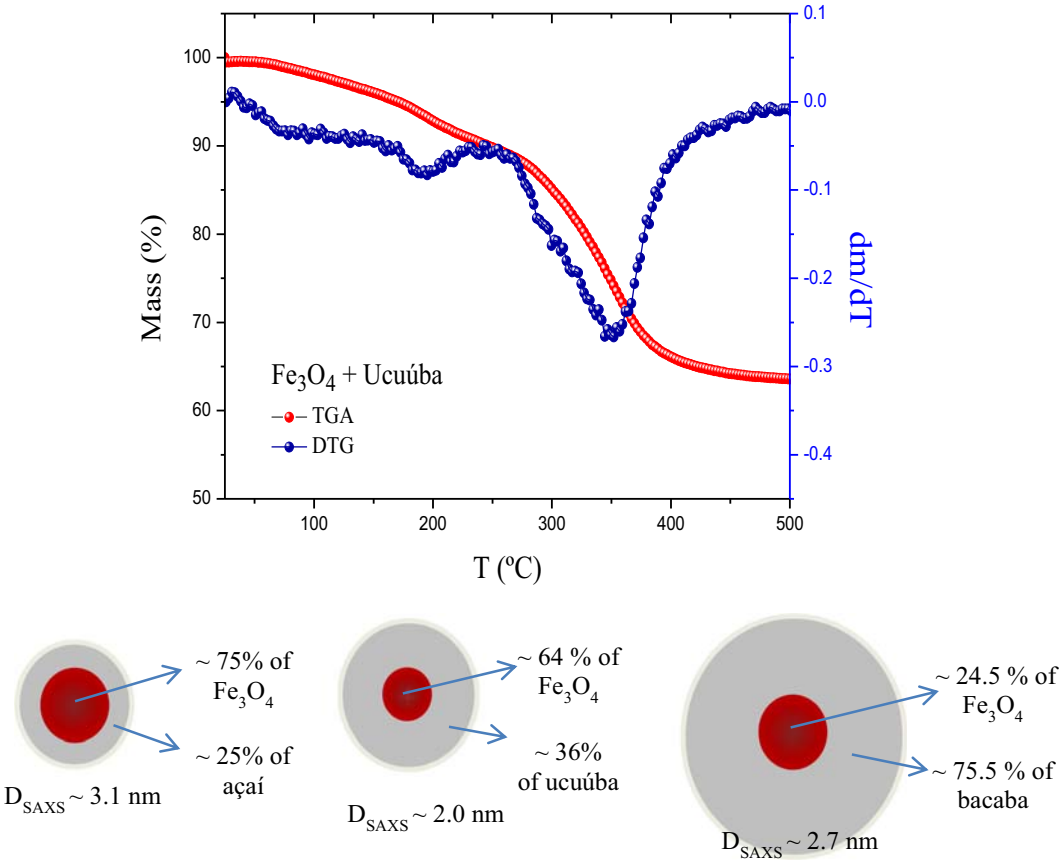

Fig. 2 Thermogravimetric analysis (TGA) and the differential thermogravimetric (DTG) curve of the Fe_3O_4 sample synthesized with ucuuba oil. The bottom panel shows a schematic drawing of the core and the shell layer containing açaí, ucuúba, and bacaba oils of the nanoparticles along with their respective NAA results for both concentrations. The average diameters (D_{SAXS}) estimated from SAXS results are also displayed

Figure 3a shows the temperature dependence of ZFC and FC magnetizations (M) measured with an applied field of H = 100 Oe for Fe_3O_4 nanoparticles coated with natural oils. All samples show essentially the same temperature profile for the ZFC and FC curves. The broad maximum of ZFC curves is usually associated with the blocking temperature (T_B) of nanoparticles (Knobel et al. 2008). This temperature separates the high-temperature superparamagnetic regime from the low temperature blocked state, where the reorientation of the particle's magnetic moment is severely restricted by the thermal energy barrier set by the magnetic anisotropy. Blocking temperatures for the three studied samples are displayed in Table 2. The behavior of the magnetization curves shown in Fig. 3 and the T_B values indicate that the particles are small with a reasonable degree of dispersion.

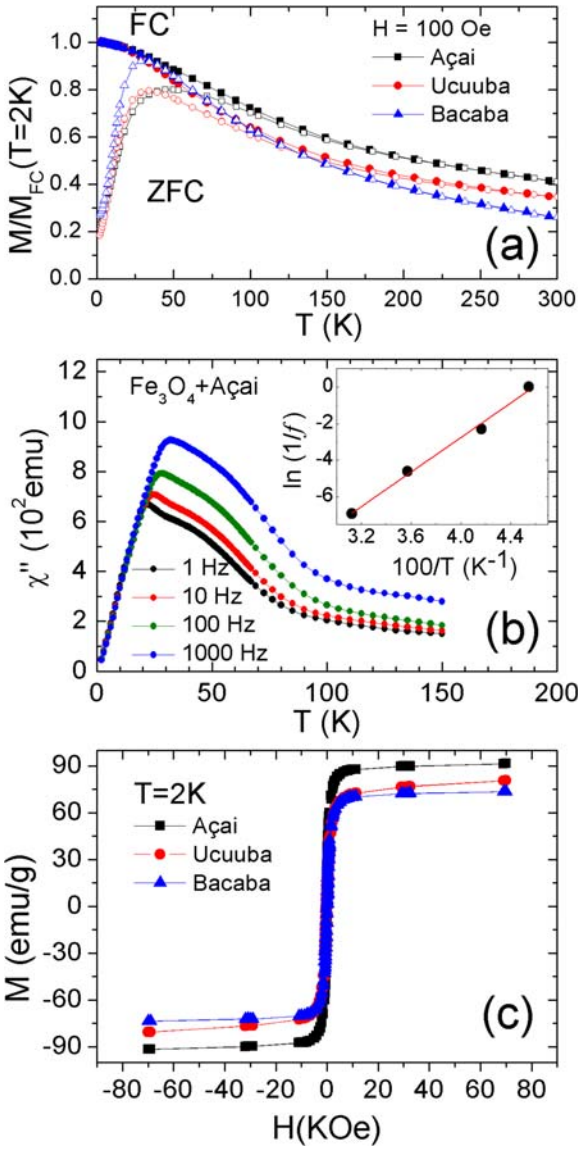

Fig. 3 **a** Temperature dependence of magnetization for Fe_3O_4 nanoparticles capped with açaí, ucuúba, and bacaba oils measured with an applied field H = 100 Oe under the zero-field-cooling (ZFC) and the field-cooling (FC) processes. Data were normalized by the FC magnetization measured at T = 2 K. **b** Imaginary component (χ") of the ac susceptibility as a function of temperature for Fe_3O_4 + açaí measured with a modulation field h_{ac} = 1 Oe changing frequency. The inset displays the Arrhenius behavior of the relaxation frequencies $1/f = (1/f_0)\exp.(E/k_BT)$. **c** Magnetization as a function of applied field H

In order to obtain the effective magnetic anisotropy of nanoparticle samples, we have used the ac susceptibility technique. The relaxation time for the thermally activated over barrier of isolated nanoparticles is given by the Néel-Brown expression (Bedanta and Kleemann 2009), $\tau = \tau_0 \exp(E/k_BT)$, where τ_0 is the so called attempt time ranging between 10^{-9} and 10^{-10} s, $E = KV$ is the uniaxial anisotropy energy barrier, K is the magnetocrystalline anisotropy, and V is the particle volume. Figure 3b displays the temperature dependence of the imaginary component χ'' of the ac susceptibility for the Fe_3O_4+ açaí sample measured with a modulation field h_{ac} = 1 Oe in the frequency range between 1 and 1000 Hz. As expected, the susceptibility shows a maximum close to T_B that shifts to higher temperatures when the frequency increases, or equivalently, with the decrease of the observation time $\tau = 1/(2\pi f)$. The data follows the Arrhenius law in the frequency domain (see the inset in Fig. 3b) from which the effective anisotropy K can be derived by calculating the slope KV/k_B of the linear fit assuming spherical particles with mean particle diameter obtained in the structural analysis.

Table 2 also displays the calculated anisotropy values for all samples. For açaí and ucuúba capped samples, the anisotropy values are within the same order of magnitude, although higher than $K = 4.74 \times 10^5$ J m^{-3} reported for 6.6 nm Fe_3O_4 nanoparticles (Caruntu et al. 2007). Nanoparticle sample synthesized with bacaba oil, on the other hand, presents an anisotropy value somewhat lower. It is also important to highlight that all these values are higher than that usually observed for bulk materials ($K_{bulk} = 1.35 \times 10^4$ J m^{-3}) (Morales et al. 1999). These results indicate that different natural oils used for capping nanoparticles influence their magnetic properties. These properties are known to be very sensitive to surface effects, which are enhanced in small particles. Among these effects, there are the possible existence of

Table 2 Structural and magnetic properties of Fe_3O_4 nanoparticle samples capped with oils extracted from the Amazon fruits açaí, ucuúba, and bacaba. D_{SAXS} are the nanoparticle diameters obtained by SAXS. K is the magnetocrystalline anisotropy determined by Arrhenius law and Stoner and Wohlfarth (S-W) model, Hc is the coercive field at 2 K, Ms is the saturation magnetization, T_B is the blocking temperature, and the organic material percentage as obtained by NAA

Fe_3O_4 sample	D_{SAXS} (nm)	K (Arrhenius) (10^5 J/m^3)	K (S-W) (10^5 J/m^3)	Hc (Oe)	Ms (emu/g)	T_B (K)	Organic material (%wt)
Açaí	3.1	4.6	3.9	343	91.4	44.7	25
Ucuúba	2.0	9.3	5.1	460	80.6	34.0	36
Bacaba	2.7	0.75	0.85	329	73.6	28.7	75

randomly oriented uncompensated surface spins for antiferromagnetic nanoparticles, the presence of canted spins or spin-glass-like behavior of the surface spins, and the occurrence of a magnetically dead layer at the surface or the enhancement of the magnetic anisotropy (Issa et al. 2013). We believe that the difference in anisotropy here observed may be ascribed to the fatty acid concentrations present in the different oils as shown in the Table 1. It is, therefore, important to notice that açaí and ucuúba oils have ~ 99.6% of saturated fatty acids whereas bacaba oil has ~ 73% of unsaturated fatty acids including a large quantity (62%) of oleic acid, which is a usual fatty acid for nanoparticles coating, stable at high temperature (around 360 °C) as reported by Zhang et al. (2007). Moreover, the lower values of K and T_B found in Fe_3O_4 + Bacaba sample when compared with Fe_3O_4 + açaí and Fe_3O_4 + ucuúba samples are an indication of a weaker interaction between the magnetic core and the outer layer of the nanoparticles capped with bacaba.

Our results indicate that fatty acids contained in oils extracted from Amazon fruits used for capping can help to produce Fe_3O_4 nanoparticles with regular and crystalline core and have a strong influence on their magnetic properties. In order to further investigate this influence, the M-H measurements were performed at T = 2 K for all samples. Figure 3c shows that the saturation magnetization (Ms) for the samples synthesized with bacaba (Ms ≈ 74 emu/g), ucuúba (Ms ≈ 81 emu/g), and açaí (Ms ≈ 91 emu/g) are very close in magnitude to that for the bulk Fe_3O_4 (Ms ≈ 90–92 emu/g).

Generally, small Fe_3O_4 nanoparticles have smaller Ms values than those here observed, because Ms is strongly dependent on the particle size (Jun et al. 2005). For instance, Ms = 37 emu/g was reported for Fe_3O_4 nanoparticles capped with oleic acid having average size around 4 nm (Parvin et al. 2004). The reduction in Ms for small nanoparticles is an open issue, and it is associated to the spin disorder in their surface layer. In magnetite, the superexchange interaction between magnetic Fe atoms is mediated by oxygen ions and, oxygen vacancies in the surface layer can lead to the Fe spin disorder resulting in Ms smaller than that for Fe_3O_4 bulk due to the large surface/volume ratio (Caruntu et al. 2007).

In fact, it has been reported in the literature that coating nanoparticles with organic and polymeric materials results in an increase of the saturation magnetization (Hou et al. 2003; Sun et al. 2004; Roca et al. 2006). On the other hand, the molecular coating absence results in defects and the oxygen lack around the iron atoms decreasing the saturation magnetization (Andrzejewski et al. 2014). Interesting results were reported by Unni et al. (2018) for small Fe_3O_4 NPs capped with oleic acid and synthesized by thermal decomposition using molecular oxygen as one of the reactive species. They show that this procedure results in single-crystalline iron oxide nanoparticles with few defects and similar physical and magnetic diameter distributions, presenting, therefore, a thin magnetically dead layer, ascribed to the presence of oxygen during synthesis. Our results then indicate that oils extracted from natural Amazon fruits with a high percentage of saturated fatty acids (açaí and ucuúba) increase Ms of small Fe_3O_4 nanoparticles, probably because saturated fatty acids influence the oxidation of iron atoms near the surface thus reducing the magnetically dead layer. This effect can be attributed to the oxygen (Unni et al. 2018) probably from the COOH functional group present in fatty acids.

The field dependence of the magnetization of all samples was measured at different temperatures in the blocked state ($T < T_B$). The inset in Fig. 4 displays the results for the Fe_3O_4+ açaí sample, which shows a clear decrease of the coercive field H_c with the increase of the

temperature. The temperature dependence of H_C in the Stoner and Wohlfarth (S-W) model is given by Stoner and Wohlfarth (1948):

$$\mathbf{H_C(T)=H_{C0}}\left[\mathbf{1-}\left(\frac{\mathbf{25k_BT}}{\mathbf{KV}}\right)^{\frac{1}{2}}\right] \quad (2)$$

This model assumes that all monodisperse particles are in the blocked state, with a random distribution of easy axis and coherent reversal of the magnetic moments. The main panel of Fig. 4 shows that the S-W model gives a good description of the data for all samples only at low temperatures ($T < 10$ K). The reason is mainly because as the temperature approaches T_B, an increasing fraction of the nanoparticles becomes unblocked and in order to improve the model, a particle size distribution needs to be taken into account. Nevertheless, the slope of the H_C vs. $T^{0.5}$ straight line fitted to experimental data at low temperature can be used to obtain an independent estimation of the effective anisotropy values *K*, which are shown in Table 2 along with *K* values obtained from susceptibility data. The increase in Hc result for Fe_3O_4+ ucuúba sample could be attributed to the quantity of fatty acid of lower carbonic chains (77.6% of C14:0 and 17% of C12:0) than those of the samples with açaí and bacaba oil (Table 1).

Results displayed in Table 2 show that nanoparticles capped with Açai and Ucuúba follow the expected behavior with the smaller particle presenting the smaller Ms and higher K. This behavior is not observed for nanoparticles capped with Bacaba that, although has an average size higher than nanoparticles capped with Ucuúba, present smaller Ms and a much smaller K. Since small nanoparticles have large surface area, the effect of spin disorder at the surface is high resulting in small Ms and high magnetic anisotropy. Our results indicate that the large amount of Bacaba capping has a stronger influence on the magnetic anisotropy.

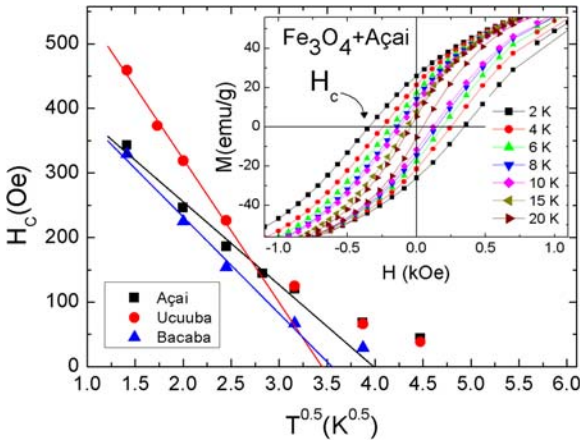

Fig. 4 Temperature dependence of the coercive field H_c obtained from the M(H) measurements for Fe_3O_4 samples. The inset shown the M(H) measurements for the Fe_3O_4+ açaí

Improvement of the magnetic properties of particles related to the coating material (organic and inorganic) has been reported in the literature, where the chemical bond of iron with chain carboxylic acids (Fe–O–C) contributes to the formation of magnetic dipoles on the surface of NPs, thus improving their magnetic properties (Knobel et al. 2008). In association with these facts, it is important to note that the oils of açaí and ucuúba have different proportions of fatty acids, which are predominantly saturated and have the carboxyl group present in their chains. On the other hand, bacaba oil has different proportions of fatty acids, however most unsaturated, as can be seen in Table 1. This difference in oil composition has certainly influence on the stabilization process and preservation of the magnetic phase of the surface layer of particles, as well as on the thickness of the capping (non-magnetic layer). Consequently, it must affect the value of the anisotropy constant, which depends on the anisotropy constant of both, the core and the surface (Lee et al. 2019). Therefore, given the different concentrations of fatty acids present in the oils used for the synthesis of Fe_3O_4 nanoparticles, these anisotropies do not follow the usual correlation with particle size since surface anisotropy would have an important contribution. In order to elucidate the surface effect, additional experiments should be carried out.

From the Spin Rotation (R(t)) spectra obtained by PAC measurements, one can determine the magnetic hyperfine field as well as the electric quadrupole hyperfine parameters that are very sensitive to the local environment around the probe nuclei reflecting, for instance, the symmetry of the nearest neighbors, possible vacancies, and electronic structure. Very similar PAC results were observed for all samples of particles capped with oils extracted from the three Amazon fruits. As an example, the R(t) spectra measured at room temperature using $^{111}In(^{111}Cd)$ as probe nuclei for Fe_3O_4 + açaí sample after synthesis and after annealing at 973 K are displayed in Fig. 5a, b, respectively. The fit of the theoretical function to the spectrum obtained after

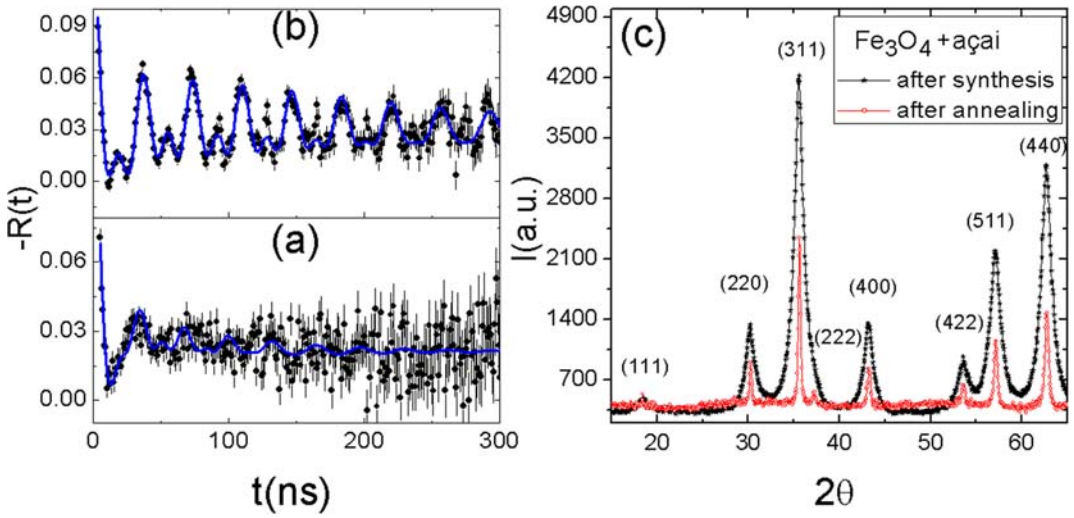

Fig. 5 PAC spectra for Fe_3O_4 + açaí sample **a** after synthesis process with ^{111}In probe nuclei and **b** after annealing at 973 K for 2.5 h with the respective **c** XRD patterns

synthesis considered that probe nuclei occupy two site fractions: one with well-defined magnetic frequency $\omega_L = 29.6$ MHz (8) and another characterized by a widely distributed (with frequency distribution $\delta \sim 50\%$) electric quadrupole frequency $\nu_Q = 270$ MHz. The Larmor frequency ω_L corresponds to a magnetic hyperfine field $B_{hf} = 12.6$ T (3). This result is a little higher than $B_{hf} = 11.8$ T (1) reported by Inglot et al. (1991) and $B_{hf} \sim 11$ T reported by Asai et al. (1985). As can be seen in Fig. 5a, the R(t) spectrum presents a strong amplitude attenuation similar to that observed by Effenberger et al. (2016) for R(t) spectra measured with ^{111}Cd in Fe_3O_4 nanoparticles capped with oleic acid.

The samples were subsequently heated at 973 K to reduce the particles coating shell (by evaporation) and increase the population of ^{111}Cd nuclei occupying Fe sites in the core of nanoparticles. PAC spectra were then measured at room temperature, and the resulting R(t) for acai-coated sample, displayed in Fig. 5b, was fitted with a model where a probe nuclei fraction with population $f = 39(3)\%$ are at substitutional Fe sites with a pure magnetic dipole interaction characterized by a well-defined (frequency distribution $\delta = 3.2(3)\%$) Larmor frequency $\omega_L = 27.3$ MHz (1). This Larmor frequency corresponds to $B_{hf} = 11.7$ T (1), equal to that observed for ^{111}Cd at substitutional Fe sites in crystalline Fe_3O_4 previously reported (Lee et al. 2019). The other probe nuclei fraction ($f = 61(3)\%$) was characterized by a broad ($\delta = 45(2)\%$) quadrupole frequency $\nu_Q =$ 137 MHz (3), which we assigned to probes at the particle surface region. Specifically, this major fraction is due to the increased surface spin disorder related to a high number of superficial iron ions with incomplete coordination environments of ^{111}Cd nuclei probe (Matos et al. 2015). The probe population values at the particle outer layer for the annealed nanoparticles, according to Effenberger et al. (2016), correspond to particle sizes around 7–8 nm.

Moreover, due to the Fe_3O_4 crystalline structure, there are two possible ^{111}Cd probe nuclei locations corresponding to the tetrahedral and octahedral sites occupied by Fe ions. The probe nuclei occupation has been controversial and, recently, ab initio calculations based on the density functional theory (DFT) were performed to elucidate ^{111}Cd probe nuclei site assignment (Sato et al. 2016). They concluded that the ^{111}Cd are located in the tetrahedral sites occupied by Fe^{3+} ions. Following these results, we have assigned the observed B_{hf} to ^{111}Cd probes at the tetrahedral sites for which the electric quadrupole interaction vanishes due to the neighboring symmetry. Furthermore, the good agreement of B_{hf} results for both samples with that for bulk Fe_3O_4 indicates that the core of the nanoparticles crystallizes in the expected structure and are free of defects. This observation is due to the results from PAC measurements that show a pure magnetic interaction (with B_{hf} agreeing with that for the bulk Fe_3O_4) for the fraction of probes assigned to replace Fe sites at the core of

nanoparticles instead of pure electric quadrupole interaction or a combined magnetic plus electric interaction, which would indicate the presence of defects (Inglot et al. 1991; Mercurio et al. 2010).

XRD patterns for Fe_3O_4 nanoparticles capped with açaí measured after synthesis and after annealing are both displayed in Fig. 5c and show that the samples present the same peaks corresponding to the cubic inverse spinel crystalline structure. As expected, it is clearly seen that after annealing, the peaks in XRD pattern are narrower than those in the pattern obtained after synthesis indicating the increase of particle size. The XRD and PAC results then indicate that the particle cores present a good crystallinity free of defects.

Conclusion

Magnetite nanoparticles were synthesized by the thermal decomposition method with oils extracted from the Amazon fruits açaí (*Euterpe oleracea*e Mart.), bacaba (Oenocarpusbacaba Mart.), and ucuúba (Virolasurinamensis). These oils were extracted by the CO_2 supercritical extraction process under low pressure and temperature and had the relative fatty acid percentages determined in their composition by gas chromatography. The characterization of all samples by XRD, PAC, and SAXS results as well as TEM images reveal, respectively, a correct crystalline structure free of defects, a small size (< 5 nm), and a regular morphology for the synthesized Fe_3O_4 nanoparticles. Measurements of their magnetic properties show that the saturation magnetization (Ms) for every measured sample is as high as that found for bulk Fe_3O_4. Therefore, the high values of Ms observed for all samples can be explained by the well-defined core structure plus the effect of the coating on the iron spins at the surface of particles, which probably was achieved due to the presence of high-saturated total fatty acid from the oils extracted from the Amazon fruits in the synthesis. The findings here reported show that the natural oils present great potential to produce good and stable nanoparticles better than those produced using only a specific fatty acid. Furthermore, oils therapeutic properties could be preserved to be used in technological and biomedical applications.

Acknowledgments The authors acknowledge the Centro de Radiofarmacia do IPEN by the supply of $^{111}InCl_3$ solution and the Coordenação de Aperfeiçoamento de Pessoal de Nível Superior (CAPES).

Authors' contributions BSC and APSS: extraction and characterization of natural oils, synthesis of Fe_3O_4 nanoparticles, characterization of synthesized nanoparticles with XRD and TEM, and preparation of samples with radioactive ^{111}In and measurements of PAC spectroscopy; MSC: synthesis of Fe_3O_4 nanoparticles, characterization of synthesized nanoparticles with XRD and TEM, and preparation of samples with radioactive ^{111}In and measurements of PAC spectroscopy; GAC: synthesis of Fe_3O_4 nanoparticles, characterization of synthesized nanoparticles with XRD and TEM, preparation of samples with radioactive ^{111}In and measurements of PAC spectroscopy and drafted the manuscript; CS: synthesis of Fe_3O_4 nanoparticles, characterization of synthesized nanoparticles with XRD and TEM, preparation of samples with radioactive ^{111}In and measurements of PAC spectroscopy and drafted the manuscript; RHHP and RNCJ: extraction and characterization of natural oils; LI and JGAR: characterization of nanoparticles with SAXS and measurements of magnetization; RSF: characterization of nanoparticles with SAXS and measurements of magnetization, drafted the manuscript; MS: determination of the Fe concentration by NAA; ITM: synthesis of Fe_3O_4 nanoparticles and preparation of samples with radioactive ^{111}In and measurements of PAC spectroscopy; and ELC: determination of the Fe concentration by NAA and preparation of samples with radioactive ^{111}In and measurements of PAC spectroscopy; AWC: drafted the manuscript and revised and organized the full final manuscript.

Funding information Financial support of this study was partially provided by the Conselho Nacional de Desenvolvimento Científico e Tecnológico (CNPq) [grant numbers 473477/2013-0, 304627/2017-8, 430060/2018–1]; Fundação de Amparo à Pesquisa do Estado de São Paulo (FAPESP) [grant numbers 2015/16191-5, 2017/50332-0].

Availability of data and materials The data and the analysis in the current work are available from the corresponding authors on reasonable request.

Authors' information N/A

Compliance with ethical standards

Competing interests The authors declare that there are no competing interests.

Abbreviations *Ms,* saturation magnetization; *XRD,* X-ray diffraction; *TEM,* transmission electron microscopy; *NAA,* neutron activation analysis; *TGA,* thermogravimetric analyzes; *SAXS,* small-angle X-ray scattering; *PAC,* perturbed angular correlation; *ASABE,* American Society of Agricultural and Biological Engineers; *ZFC,* zero-field-cooled; *FC,* field-cooled; *DTG,* differential thermogravimetric

References

Abadio Finco FDB, Kammerer DR, Carle R, Tseng W-H, Boser S, Graeve L (2012) Antioxidant activity and characterization of phenolic compounds from Bacaba (Oenocarpus bacaba Mart.) fruit by HPLC-DAD-MSn. J Agric Food Chem 60: 7665–7673. https://doi.org/10.1021/jf3007689

Ahmed S, Saifullah AM, Swami BL, Ikram S (2016) Green synthesis of silver nanoparticles using *Azadirachta indica* aqueous leaf extract. J Radiat Res Appl Sci 9:1–7. https://doi.org/10.1016/j.jrras.2015.06.006

American Society of Agricultural and Biological Engineers, ANSI/ASAE S319: method of determining and expressing fineness of feed materials by sieving, St. Joseph: ASABE, 1998, 547

Andrzejewski B, Bednarski W, Kazmierczak M, Lapinski A, Pogorzelec-Glaser K, Hilczer B, Jurga S, Nowaczyk G, Zaleski K, Matczak M, Leska B, Pankiewicz R, Kepinski L (2014) Magnetization enhancement in magnetite nanoparticles capped with alginic acid. Compos Part B Eng 64:147–154. https://doi.org/10.1016/j.compositesb.2014.04.022

Asai K, Okada T, Sekizawa H (1985) TDPAC of γ-rays emitted from ^{111}Cd(←^{111}In) in Fe_3O_4. J Phys Soc Jpn 54:4325–4330. https://doi.org/10.1143/JPSJ.54.4325

Barbeta VB, Jardim RF, Kiyohara PK, Effenberger FB, Rossi LM (2010) Magnetic properties of Fe_3O_4 nanoparticles coated with oleic and dodecanoic acids. J Appl Phys 107:073913-1–073913-7. https://doi.org/10.1063/1.3311611

Batista CCR, Oliveira MS, Araújo ME, Rodrigues AMC, Botelho JRS, Souza Filho APS, Machado NT, Carvalho Junior RN (2016) Supercritical CO_2 extraction of açaí (*Euterpe oleracea*) berry oil: global yield, fatty acids, allelopathic activities, and determination of phenolic and anthocyanins total compounds in the residual pulp. J Supercrit Fluids 107: 364–369. https://doi.org/10.1016/j.supflu.2015.10.006

Bedanta S, Kleemann W (2009) Supermagnetism. J Phys D Appl Phys 42:013001. https://doi.org/10.1088/0022-3727/42/1/013001

Bosch-Santos B, Carbonari AW, Cabrera-Pasca GA, Saxena RN, Freitas RS (2015) The magnetic behavior of the intermetallic compound $NdMn_2Ge_2$ studied by magnetization and hyperfine interactions measurements. J Appl Phys 117:17E304-1–17E304-4. https://doi.org/10.1063/1.4907330

Brollo MEF, López-Ruiz R, Muraca D, Figueroa SJA, Pirota KR, Knobel M (2014) Compact Ag@Fe_3O_4 Core-shell nanoparticles by means of single-step thermal decomposition reaction. Sci Rep 4:6839. https://doi.org/10.1038/srep06839

Caruntu D, Caruntu G, O'Connor CJ (2007) Magnetic properties of variable-sized Fe_3O_4 nanoparticles synthesized from non-aqueous homogeneous solutions of polyols. J Phys D Appl Phys 40:5801–5809. https://doi.org/10.1088/0022-3727/40/19/001

Carvalho AA, Galdino PM, Nascimento MV, Kato MJ, Valadares MC, Cunha LC, Costa EA (2010) Antinociceptive and antiinflammatory activities of grandisin extracted from Virola surinamensis. Phytother Res 24:113–118. https://doi.org/10.1002/ptr.2882

Chen Y, Song B, Liv LL, Xue J (2014) Fe_3O_4 nanoparticles embedded in uniform mesoporous carbon spheres for superior high-rate battery applications. Adv Funct Mater 24:319–326. https://doi.org/10.1002/adfm.201300872

Corrêa EL, Bosch-Santos B, Freitas RS, Potiens MPA, Saiki M, Carbonari AW (2018) Synthesis and atomic scale characterization of Er_2O_3 nanoparticles: enhancement of magnetic properties and changes in the local structure. Nanotechnology 29:205704.1–205704.20570410. https://doi.org/10.1088/1361-6528/aab3f8

Costa WA, Oliveira MS, Silva MP, Cunha VMB, Pinto RHH, Bezerra FWF, Carvalho Junior RN (2017) Açaí (*Euterpe oleracea*) and Bacaba (*Oenocarpus bacaba*) as functional food. In: Shiomi N (ed) Superfood and Functional Food - An Overview of Their Processing and Utilization Publisher. InTech, pp 155–172. https://doi.org/10.5772/65881

Cuong ND, Hoa TT, Khieu DQ, Lam TD, Hoa ND, Hieu NV (2012) Synthesis, characterization, and comparative gas-sensing properties of Fe_2O_3 prepared from Fe_3O_4 and Fe_3O_4-chitosan. J Alloys Compd 523:120–126. https://doi.org/10.1016/j.jallcom.2012.01.117

Da Rocha Filho GN, Bentes MHS, Brodzki D, Djega-Mariadassou G (1992) Catalytic conversion of *Hevea brasiliensis* and *Virola sebifera* oils to hydrocarbons oils. J Am Oil Chem Soc 69:266–271. https://doi.org/10.1007/BF02635899

De Soete D, Gijbels R, Hoste J (1972) Neutron activation analysis. Wiley, New York

Dogra R, Junqueira AC, Saxena RN, Carbonari AW, Mestnik-Filho J, Moralles M (2001) Hyperfine interaction measurements in LaCrO3 and LaFeO3 perovskites using perturbed angular correlation spectroscopy. Phys Rev B 63:224104-1–224104-9. https://doi.org/10.1103/PhysRevB.63.224104

Effenberger FB, Carbonari AW, Rossi LM (2016) The influence of 1, 2-alkanediol on the crystallinity of magnetite nanoparticles. J Magn Magn Mater 417:49–55. https://doi.org/10.1016/j.jmmm.2016.05.028

Fregonesi A, Scanavez C, Santos L, De Oliveira A, Roesler R, Escudeiro C, Moncayo P, De Sanctis D, Gesztesi JL (2009) Brazilian oils and butters: the effect of different fatty acid chain composition on human hair physiochemical properties. J Cosmet Sci 60:273–280. https://doi.org/10.1111/j.1468-2494.2010.00534_16.x

Gordon A, Cruz APG, Cabral LMC, Freitas SC, Dib Taxi CMA, Donangelo CM, Mattietto RA, Friedrich M, Matta VM, Marx F (2012) Chemical characterization and evaluation of antioxidant properties of Açaí fruits (*Euterpe oleraceae* Mart.) during ripening. Food Chem 133:256–263. https://doi.org/10.1016/j.foodchem.2011.11.150

Guivar JAR, Fernandes EGR, Zucolotto V (2015) A peroxidase biomimetic system based on Fe_3O_4 nanoparticles in non-enzymatic sensors. Talanta 141:307–314. https://doi.org/10.1016/j.talanta.2015.03.017

Hiruma-Lima CA, Batista LM, Almeida ABA, Magri LP, Santos LC, Vilegas W, Brito ARMS (2009) Antiulcerogenic action of ethanolic extract of the resin from *Virola surinamensis* Warb. (Myristicaceae). J Ethnopharmacol 122:406–409. https://doi.org/10.1016/j.jep.2008.12.023

Holderness J, Schepetkin IA, Freedman B, Kirpotina LN, Quinn MT, Hedges JF, Jutila MA (2011) Polysaccharides isolated from açaí fruit induce innate immune responses. PLoS One 6(2):e17301.1–e1730114. https://doi.org/10.1371/journal.pone.0017301

Hou Y, Yu J, Gao S (2003) Solvothermal reduction synthesis and characterization of superparamagnetic magnetite nanoparticles. J Mater Chem 13:1983–1987. https://doi.org/10.1039/B305526D

Hussain I, Singh NB, Singh A, Singh H, Singh SC (2016) Green synthesis of nanoparticles and its potential application. Biotechnol Lett 38:545–560. https://doi.org/10.1007/s10529-015-2026-7

Iizumi M, Koetzle TF, Shirane G, Chikazumi S, Matsui M, Todo S (1982) Structure of magnetite (Fe_3O_4) below the Verwey transition temperature. Acta Cryst B38:2121–2133. https://doi.org/10.1107/S0567740882008176

Inglot Z, Wiarda D, Lieb KP, Wenzel T, Uhrmacher M (1991) Defects in $Fe_{1-x}O$ and the $Fe_{1-x}O$ to Fe_3O_4 phase transition studied by the perturbed angular correlation method. J Phys Condens Matter 3:4569–4585. https://doi.org/10.1088/0953-8984/3/25/006

Iravani S (2011) Green synthesis of metal nanoparticles using plants. Green Chem 13:2638–2650. https://doi.org/10.1039/C1GC15386B

Issa B, Obaidat IM, Albiss BA, Haik Y (2013) Magnetic nanoparticles: surface effects and properties related to biomedicine applications. Int J Mol Sci 14:21266–21305. https://doi.org/10.3390/ijms141121266

Jiao M, Zeng J, Jing L, Liu C, Gao M (2015) Flow synthesis of biocompatible Fe_3O_4 nanoparticles: insight into the effects of residence time, fluid velocity, and tube reactor dimension on particle size distribution. Chem Mater 27:1299–1305. https://doi.org/10.1021/cm504313c

Jun Y-W, Huh Y-M, Choi J-S, Lee J-H, Song H-T, Kim S, Yoon S, Kim K-S, Shin JS, Suh JS, Cheon J (2005) Nanoscale size effect of magnetic nanocrystals and their utilization for cancer diagnosis via magnetic resonance imaging. J Am Chem Soc 127:5732–5733. https://doi.org/10.1021/ja0422155

Knobel M, Nunes WC, Socolovsky LM, De Biasi E, Vargas JM, Denardin JC (2008) Superparamagnetism and other magnetic features in granular materials: a review on ideal and real systems. J Nanosci Nanotechnol 8:2836–2857. https://doi.org/10.1166/jnn.2008.15348

Lee K, Lee S, Ahn B (2019) Understanding high anisotropic magnetism by ultrathin shell layer formation for magnetically hard–soft core–shell nanostructures. Chem Mater 31:728–736. https://doi.org/10.1021/acs.chemmater.8b03591

Liao H, Shelor CP, Chen Y, Sabaa-Srur AUO, Smith RE, Dasgupta PK (2013) Anion composition of açaí extracts. J Agric Food Chem 61:5928–5935. https://doi.org/10.1021/jf4014185

Lopes NP, Blumenthal EEA, Cavalheiro AJ, Kato MJ, Yoshida M (1996) Lignans, γ-lactones and propiophenones of *Virola surinamensis*. Phytochemistry 43:1089–1092. https://doi.org/10.1016/S0031-9422(96)00408-6

Lopes NP, Kato MJ, Yoshida M (1999) Antifungal constituents from roots of Virola surinamensis. Phytochemistry 51:29–33. https://doi.org/10.1016/S0031-9422(98)00709-2

Matos IT, Bosch-Santos B, Cabrera-Pasca GA, Carbonari AW (2015) Magnetic behavior of La-doped Fe_3O_4 studied by perturbed angular correlation spectroscopy with ^{111}Cd and ^{140}Ce. J Appl Phys 117:17D511-1–17D511-4. https://doi.org/10.1063/1.4916023

Mercurio ME, Carbonari AW, Cordeiro MR, Saxena RN, D'Agostino LZ (2010) Local investigation of hyperfine interactions in pure and Co-doped ZnO. J Magn Magn Mater 322:1195–1197. https://doi.org/10.1016/j.jmmm.2009.06.051

Morales MP, Veintemillas-Verdaguer S, Montero MI, Serna CJ, Roig A, Casas LI, Martínez B, Sandiumenge F (1999) Surface and internal spin canting in γ-Fe_2O_3 nanoparticles. Chem Mater 11:3058–3064. https://doi.org/10.1021/cm991018f

Nemala H, Thakur JS, Naik VM, Vaishnava PP, Lawes G, Naik R (2014) Investigation of magnetic properties of Fe_3O_4 nanoparticles using temperature dependent magnetic hyperthermia in ferrofluids. J Appl Phys 116:034309-1–034309-6. https://doi.org/10.1063/1.4890456

Oliveira FCC, Effenberger FB, Sousa MH, Jardim RF, Kiyohara PK, Dupont J, Rubim JC, Rossi LM (2011) Ionic liquids as recycling solvents for the synthesis of magnetic nanoparticles. Phys Chem Chem Phys 13:13558–13564. https://doi.org/10.1039/C1CP21518C

O'Neill HSC, Dollase WA (1994) Crystal structures and cation distributions in simple spinels from powder XRD structural refinements: $MgCr_2O_4$, $ZnCr_2O_4$, Fe_3O_4 and the temperature dependence of the cation distribution in $ZnAl_2O_4$. Phys Chem Miner 20:541–555. https://doi.org/10.1007/BF00211850

Parvin K, Ma J, Ly J, Sun XC, Nikles DE, Sun K, Wang LM (2004) Synthesis and magnetic properties of monodisperse Fe_3O_4 nanoparticles. J Appl Phys 95:7121–7123. https://doi.org/10.1063/1.1682783

Pérez-Dieste V, Castellini OM, Crain JN, Eriksson MA, Kirakosian A, Lin J-L, McChesney JL, Himpsel FJ, Black CT, Murray CB (2003) Thermal decomposition of surfactant coatings on Co and Ni nanocrystals. Appl Phys Lett 83:5053–5055. https://doi.org/10.1063/1.1633971

Pistone A, Piperno A, Iannazzo D, Donato N, Latino M, Spadaro D, Neri G (2013) Fe_3O_4-MWCNT-PhCOOH composites for ammonia resistive sensors. Sens Actuators B Chem 186:333–342. https://doi.org/10.1016/j.snb.2013.06.027

Ramirez FEN, Cabrera-Pasca GA, Mestnik-Filho J, Carbonari AW, Souza JA (2015) Magnetic and transport properties assisted by local distortions in $Bi_2Mn_4O_{10}$ and $Bi_2Fe_4O_9$ multiferroic compounds. J Alloys Compd 651:405–413. https://doi.org/10.1016/j.jallcom.2015.08.165

Ren X, Chen H, Yang V, Sun D (2014) Iron oxide nanoparticle-based theranostics for cancer imaging and therapy. Front Chem Sci Eng 8:253–264. https://doi.org/10.1007/s11705-014-1425-y

Roca AG, Morales MP, Grady KO, Serna CJ (2006) Structural and magnetic properties of uniform magnetite nanoparticles prepared by high temperature decomposition of organic precursors. Nanotechnology 17:2783–2788. https://doi.org/10.1088/0957-4484/17/11/010

Rodrigues AMC, Darnet S, Silva LHM (2010) Fatty acid profiles and tocopherol contents of buriti (*Mauritia flexuosa*), patawa (*Oenocarpus bataua*), tucuma (*Astrocaryum vulgare*), mari (*Poraqueiba paraensis*) and inaja (*Maximiliana maripa*) fruits. J Braz Chem Soc 21:2000–2004. https://doi.org/10.1590/S0103-50532010001000028

Sahoo Y, Pizem H, Fried T, Golodnitsky D, Burstein L, Sukenik CN, Markovich G (2001) Alkyl phosphonate/phosphate coating on magnetite nanoparticles: a comparison with fatty acids. Langmuir 17:7907–7911. https://doi.org/10.1021/la010703+

Sales TSN, Cavalcante FHM, Bosch-Santos B, Pereira LFD, Cabrera-Pasca GA, Freitas RS, Saxena RN, Carbonari AW (2017) Stable tetragonal phase and magnetic properties of Fe-doped HfO_2 nanoparticles. AIP Adv 7:056315-1–056315-6. https://doi.org/10.1063/1.4976583

Sato W, Ida T, Komatsuda S, Fujisawa T, Takenaka S, Ohkubo Y (2016) Thermal stability of nonmagnetic Cd and in impurities in Fe_3O_4. J Appl Phys 120:145104. https://doi.org/10.1063/1.4964694

Schauss AG, Wu X, Prior RL, Ou B, Patel D, Huang D, Kababick JP (2006) Phytochemical and nutrient composition of the freeze-dried Amazonian palm berry, Euterpe oleraceae Mart. (Açaí). J Agric food Chem 54:8598–8603. https://doi.org/10.1021/jf060976g

Sena C, Costa MS, Muñoz EL, Cabrera-Pasca GA, Pereira LFD, Mestnik-Filho J, Carbonari AW, Coaquira JAH (2015) Charge distribution and hyperfine interactions in the vicinity of impurity sites in In_2O_3 doped with Fe, Co, and Ni. J Magn Magn Mater 387:165–178. https://doi.org/10.1016/j.jmmm.2015.03.092

Shen M, Cai H, Wang X, Cao X, Li K, Wang SH, Guo R, Zheng L, Zhang G, Shi X (2012) Facile one-pot preparation, surface functionalization, and toxicity assay of APTS-coated iron oxide nanoparticles. Nanotechnology 23:105601.1–105601.10560110. https://doi.org/10.1088/0957-4484/23/10/105601

Soares BMC, Gamarra FMC, Paviani LC, Gonçalves LAG, Cabral FA (2007) Solubility of triacylglycerols in supercritical carbon dioxide. J Supercrit Fluids 43:25–31. https://doi.org/10.1016/j.supflu.2007.03.013

Stoner EC, Wohlfarth EP (1948) A mechanism of magnetic hysteresis in heterogeneous alloys Phil. Trans. Roy. Soc. London A, 240:599-642. https://doi.org/10.1098/rsta.1948.0007; Reprinted by IEEE Trans Magn (1991) 27:3475-3518. https://doi.org/10.1109/TMAG.1991.1183750

Sun S, Zeng H, Robinson DB, Raoux S, Rice PM, Wang SX, Li G (2004) Monodisperse MFe_2O_4 (M = Fe, Co, Mn) nanoparticles. J Am Chem Soc 126:273–279. https://doi.org/10.1021/ja0380852

Svergun DI (1992) Determination of the regularization parameter in indirect-transform methods using perceptual criteria. J Appl Crystallogr 25:495–503. https://doi.org/10.1107/S0021889892001663

Teixeira-Neto AA, Izumi CMS, Temperini MLA, Ferreira AMC, Constantino VRL (2012) Hybrid materials based on Smectite clays and nutraceutical anthocyanins from the Açaí fruit. Eur J Inorg Chem 32:5411–5420. https://doi.org/10.1002/ejic.201200702

Uhrmacher M (2011) Can PAC measurements be used to investigate defects in nanostructures? Defects Diffus Forum 311:105–133. https://doi.org/10.4028/www.scientific.net/DDF.311.105

Unni M, Uhl A, Savliwala S, Savitzky BH, Dhavalikar R, Garraud N, Arnold DP, Kourkoutis LF, Andrew J, Rinaldi C (2018) Thermal decomposition synthesis of iron oxide nanoparticles with diminished magnetic dead layer by controlled addition of oxygen. ACS Nano 11:2284–2303. https://doi.org/10.1021/acsnano.7b00609

Yamaguchi KKL, Pereira LFR, Lamarão CV, Lima ES, Da Veiga Junior VF (2015) Amazon acai: chemistry and biological activities: a review. Food Chem 179:137–151. https://doi.org/10.1016/j.foodchem.2015.01.055

Yuan Y, Rende D, Altan CL, Bucak S, Ozisik R, Borca-Tasciuc D-A (2012) Effect of surface modification on magnetization of Iron oxide nanoparticle colloids. Langmuir 28:13051–13059. https://doi.org/10.1021/la3022479

Zhang L, He R, Hong-Chen G (2006) Oleic acid coating on the monodisperse magnetite nanoparticles. Appl Surf Sci 253:2611–2617. https://doi.org/10.1016/j.apsusc.2006.05.023

Zhang Y, Zeng G-M, Tang L, Huang D-L, Jiang X-Y, Chen Y-N (2007) A hydroquinone biosensor using modified core–shell magnetic nanoparticles supported on carbon paste electrode. Biosens Bioelectron 22:2121–2126. https://doi.org/10.1016/j.bios.2006.09.030